In Situ Observation of Heterogeneous Growth of CdSe Quantum Dots: Effect of Indium Doping on the Growth Kinetics

Christopher Tuinenga,[†] Jacek Jasinski,[‡] Takeo Iwamoto,[§] and Viktor Chikan[†,*]

[†]Department of Chemistry, Kansas State University, Manhattan, Kansas 66506-3701, [‡]School of Engineering, University of California, Merced, 5200 North Lake Road, Merced, California 95343, and [§]Department of Biochemistry, Kansas State University, Manhattan, Kansas 66506

ABSTRACT In this study, the heterogeneous growth of CdSe nanoparticles is reported by using *in situ* fluorescence spectroscopy. In the heterogeneous growth regime, nanoparticles with well-defined and very different sizes can coexist in the solution. The average size and size distribution of the nanoparticles is primarily not controlled by the usual focusing—defocusing (Ostwald ripening) of particles, rather by the formation of "magic" sized particles. In these studies, the effects of indium doping from indium chloride on the growth kinetics, size, size distribution, as well as the quantum yield of the various particles in the growth solution is investigated. Specifically, it is shown that the indium atoms accelerate the dissolution of the magic sized CdSe nanoparticles, while the chloride ions seem to stabilize the magic size particles. The present result will help to improve the understanding of how a dopant atom can affect the growth kinetics of semiconductor nanoparticles.

KEYWORDS: doping · growth kinetics · nanoparticle · magic size · heterogeneous growth

Semiconductor nanocrystals have garnered significant attention due to their size-dependant optical properties,[1] shape control,[2,3] and the formation of core/shell particles.[4,5] Due to their wide absorption cross sections and narrow emission bands, CdSe quantum dots (QDs) have attracted interest in fields of photosensitizers[6] and biomedical imaging.[7]

Traditionally, the optical and electronic properties of CdSe QDs are controlled by the size of the particle. Doping provides an alternative route to controlling the electronic properties of quantum dots without changing the size and has begun to attract attention.[8] Doping can be achieved in two ways: electrochemical or by incorporation of impurity atoms. Electrochemical doping, or charging, has already been reported,[9] while doping in the form of introducing impurity atoms was predicted as difficult[10] due to the phenomenon of self-purification.[11] Most reported results of doping in CdSe QDs have been restricted to the incorporation of transition metals in the 2+ state[12,13] that replace Cd^{2+} and seek to exploit the magnetic properties of the dopant atom's unpaired electrons. Few reports exist concerning the doping of CdSe quantum dots to form shallow, hydrogen-like, acceptor or donor levels (n-type and p-type conduction, respectively). Indium is routinely used in n-type doping of bulk CdSe[14] and in CdSe thin films.[15] Indium is ideal for doping CdSe because the atomic radii of Cd and In are equal, reducing lattice strain when In^{3+} replaces Cd^{2+}. Encouraged by reports of successful incorporation of Mg^{2+} into CdSe QDs using $MgCl_2$ and the $Li_4[Cd_{10}Se_4(SPh)_{16}]$,[16] we began to explore the effects of $InCl_3$ on CdSe QDs grown with this single source precursor method.[17]

Quantum dots containing acceptor and donor levels can be used to create quantum confined p−n junctions capable of improved charge carrier separation over bulk semiconductors. These quantum p−n junctions can lead to improved efficiency in solar cells, serve as a "bottom-up" platform for microchip technology, and increase sensitivity of photodetectors. CdSe has become a benchmark system of study in the quantum confined size region and, therefore, is an ideal system not only to develop a quantum p−n junction but also to be a general model of how doping effects quantum dots.

Although many studies focused on the preparation of doped QDs, much less effort has been committed to explore the role of dopant atoms on the growth kinetics. This work has three important contributions, which clarify this role. First, a heterogeneous growth regime of the CdSe QDs is reported here, which significantly differs from the usual focusing−defocusing regime of the nanoparticle growth.[18] During the early growth stages, the presence of two very different sized CdSe nanoparticles is observed. Second, *in situ* fluorescence spectroscopy is

*Address correspondence to chikan@ksu.edu.

Received for review November 19, 2007 and accepted May 16, 2008.

Published online June 20, 2008.
10.1021/nn700377q CCC: $40.75

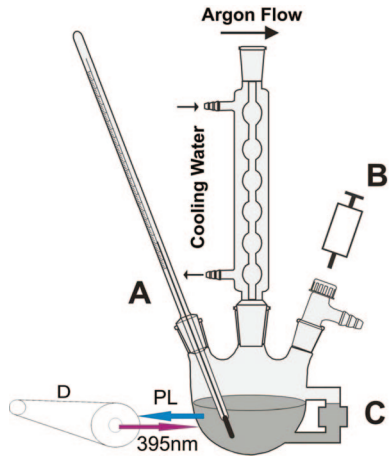

Figure 1. Experimental setup for collecting *in situ* absorbance and *in situ* photoluminescence. (A) Temperature monitor, (B) injection port, and (C) cuvette directly attached to the reaction vessel for *in situ* monitoring. Fluorescence monitoring is carried out by a fiber optic Raman probe (D).

described and demonstrated as a practical tool to study the growth kinetics as well as the defects of the semiconductor QDs during growth. Third, it is shown that various forms of the dopant precursor affect the success of doping as well as the nanoparticle growth kinetics. In addition, the effect of the dopant on the growth kinetics can be different at different temperatures as demonstrated by the experimental data.

RESULTS AND DISCUSSIONS

***In Situ* Observation of Photoluminescence.** The experimental setup used to monitor the photoluminescence spectrum during growth is shown in Figure 1. The setup is identical to the one reported previously[19] with the addition of a surface Raman probe. The surface Raman probe is equipped with a LED with emission centered at 395 nm. The probe is adjusted to allow for maximum collection of the excitation light with the narrowest peak.

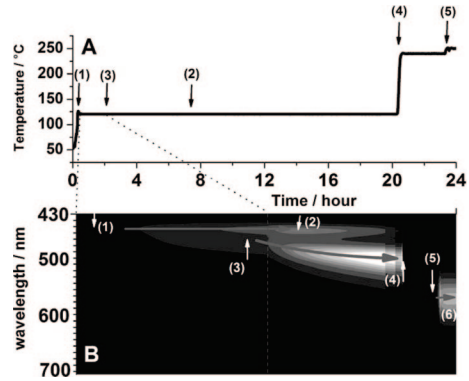

Figure 2. (A) Temperature profile of a typical synthesis. The arrows and numbers correspond to the same numbers in the density plot of emission (B). (C) Absorbance and emission profile of the heterogeneous mixture after stirring overnight at 120 °C along with the measure fwhm of the emission peaks. Note the fwhm of the magic size is half that of the larger size.

Heterogeneous Growth of CdSe Quantum Dots. Figure 2 shows the evolution of photoluminescence with respect to time during the growth phase of the synthesis of CdSe quantum dots. Figure 2A is the temperature profile, while Figure 2B is the compiled photoluminescence spectra over the growth phase. As the temperature is slowly increased to 120 °C, the $Li_4[Cd_{10}Se_4(SPh)_{16}]$ cluster decomposes and a single peak develops and shifts to the red until reaching 450 nm. After a short time, a second peak begins to grow out of the first and shifts further to the red. The arrows correspond to (1) the emergence of the first peak, (2) the maximum fluorescence of the first peak, (3) the emergence of the second peak, and (4) the second peak's maximum fluorescence. Arrow 5 denotes the photoluminescence peak position after 3 h of growth at 240 °C. During this growth, the photoluminescence is greatly reduced and reappears upon cooling to lower temperatures. When the solution is heated, the photoluminescence is quenched due to both the accelerated formation of structural and surface defects in the nanoparticles and increased phonon population at higher temperature. Arrow 6 denotes the emission peak position during the growth of the ZnS shell material. During the growth of the ZnS shell, a red shift is observed in the emission spectrum of the CdSe core and the intensity of the emission begins to increase.

As the reaction progresses, the second peak becomes more intense than the first one. After several hours, the maximum intensity at 460 nm is reached, at which point emission begins to decrease. While the emission centered at 460 nm begins to diminish, the emission from the second peak begins to steadily increase. This suggests that the smaller "magic size" family of QDs is consumed, facilitating the growth of larger particles. This differs from "traditional" Ostwald ripening in two ways: (1) the growth is not continuous from one size to the next, and there is only the peak at 450 nm and then the second peak around 500 nm and nothing in between; and (2) the final purified photoluminescence spectra show a non-Gaussian size distribution, as shown in Figure 3A. Ostwald ripening occurs during colloid growth when the concentration of monomers drops below the supersaturation limit. Without substantial monomer concentration, smaller colloids decompose in order to provide monomers that enable the larger particles in solution to grow. When Ostwald ripening does occur, there is a continuous growth of the colloid sample, and the absorbance and photoluminescence peaks shift smoothly to the red end of the spectrum. In the case of heterogeneous growth as described here, there is no smooth shift from blue to red, rather there is a gap between the two groups of particles. Inside this "growth gap", there is no evidence for the existence of any particles. Simply put, no QD sizes can exist in significant concentration between the group at 460 nm and the group at ~500 nm under

these growth conditions. While Ostwald ripening widens the size distribution of the QD ensemble, the distribution remains a smooth Gaussian distribution.

The absorbance and emission spectra of the magic size nanocluster observed in these experiments are represented in Figure 3A. Two significant observations can be made from Figure 3A: (1) the magic size nanocluster's (MSNC) emission spectrum is asymmetrical, and (2) the magic size cluster exhibits surface trap emission in the range of 500−600 nm. The tailing of the emission spectrum toward the red is generally considered more characteristic of molecular fluorophors than quantum dots.

In an effort to better understand the formation of the MSNC, matrix-assisted laser desorption ionization time of flight (MALDI-TOF) mass spectrometry was preformed on purified solution of the MSNC. As seen in Figure 3C, there are two peaks shown in the blown up inset where the first corresponds to $(CdSe)_{25}$ at 4784 mass units and a second and more intense peak at 4800 mass units corresponding to $(CdSe)_{25}$ + O. Using the established densities for both wurtzite and zinc blende crystal structures and idealizing the nanocluster as a perfect sphere, a radius of 0.49 nm is obtained for wurtzite and 0.495 nm for zinc blende. It can therefore be concluded that regardless of crystal structure the magic size cluster reported here has a diameter of ~1 nm. The absorption peak position of 435 nm corresponds to particles larger than 1 nm in diameter, so this $(CdSe)_{25}$ particle is not likely to be the magic sized nanocluster observed during our synthesis. It is possible that this particle size is the result of fragmentation of larger particles caused by the laser.

We propose that the more intense peak at 4800 mass units is the 1 nm $(CdSe)_{25}$ cluster with an oxygen ion coordinated to its surface. A this time, it is not possible to determine if the oxygen is present in the synthetic system or is a result of exposure to oxygen during purification and during the MALDI experiment.

Magic sized nanoclusters are generally explained by two phenomenon. The first is a closed-shell structure[20] where the surface atoms obtain a closed valence shell structure. This generally occurs in the zinc blende crystal structure because of the tetrahedral bonding scheme.[20] In this state, the dangling bonds of the surface atoms are either minimized or absent. The second explanation for MSNC is the overall energy of the particles becomes minimized.[21,22] With the overall energy minimized, the particles cease to grow and the size distribution is focused to the magic size in order to lower the energy of the collective system. In the case of heterogeneous growth, a magic size cluster is obtained, but due to the high monomer concentration, additional monomers are added to the surface—most likely at high energy surface sites such as corners and edges. This addition breaks the closed shell configuration, and the particles grow to the next most stable size under

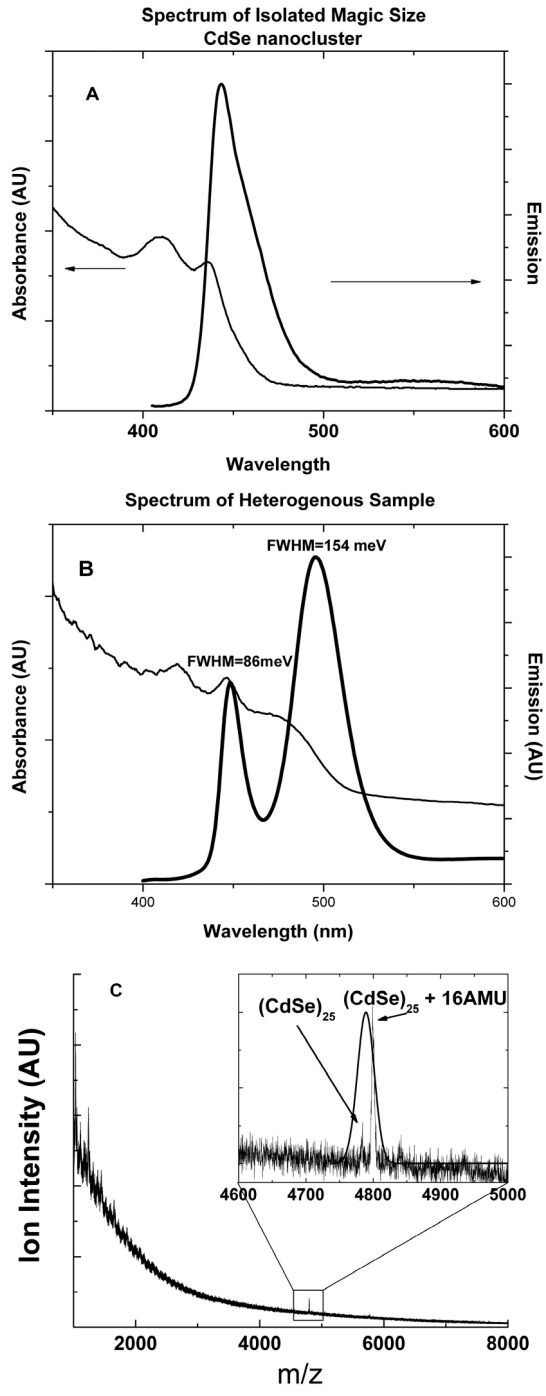

Figure 3. (A) Absorbance and photoluminescence spectra of $(CdSe)_{25}$ magic size nanocluster. (B) Absorbance and photoluminescence spectrum of quantum dots present at the end of the low-temperature growth phase. (C) MALDI spectrum showing a peak at ~4800 mass units. Inset: $(CdSe)_{25}$ and $(CdSe)_{25}$ + O peaks.

the reaction conditions. Interestingly, this event only takes place at the early stage of the growth. In the case presented, the 450 nm size represents the first closed shell configuration to which an additional monomer unit is added. Upon losing the closed shell and the stability that accompanies it, the particle behaves as a "normal" particle and continues to grow until mono-

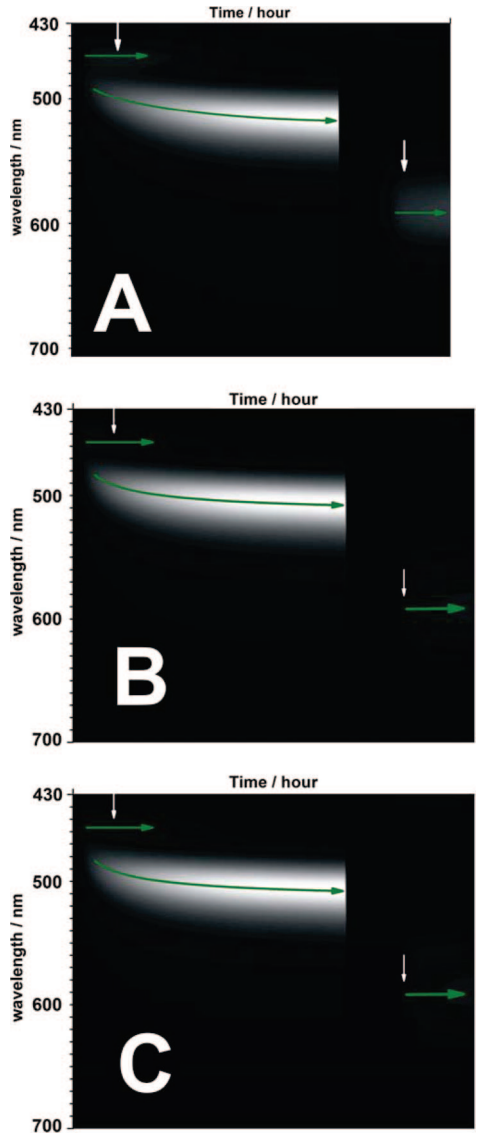

Figure 4. *In situ* photoluminescence *versus* time plot of quantum dots doped with $InCl_3$: 5 (A), 10 (B), and 15 mol % (C) with respect to cadmium. The peak attributed to the magic size nanocluster vanishes quicker with increasing indium load, and the emission from the final core−shell product diminishes with increasing load, as well.

mers are unavailable. The size distribution of the magic sized nanoparticle at 450 nm can be estimated from the fwhm of the emission peak. Both high-temperature photoluminescence data and the emission from purified samples show approximately 80 meV fwhm, which agrees well with the best observed emission peak width in the literature.[23]

Effects of Indium Chloride on Growth. Varying the concentration of indium chloride in the solution changes the heterogeneous growth kinetics observed in the experiments where no indium chloride is added. Figure 4 shows the compiled emission spectra of experiments with (a) 5 mol %, (b) 10 mol %, and (c) 15 mol % of indium chloride with respect to the number of moles of cadmium. The first change produced by the addition of the doping agent is that the time to reach the first peak's maximum emission decreases as the amount of indium increases (15% > 10% > 5%). There are two possible explanations for this phenomenon: (a) the presence of indium chloride in solution activates the CdSe monomers, or (b) the indium chloride activates the quantum dots' surface. With respect to (b), it can be argued that, when an atom of indium or chlorine bonds to the surface of the particle, the surface energy is increased, making the surface more susceptible to growth. The second difference the addition of $InCl_3$ produces is that the first peak is eventually consumed at the benefit of the second peak, indicating that adding indium chloride activates Ostwald ripening at early stages of growth. This will be discussed below. Third, when the ZnS shell is added and indium chloride is present, the photoluminescence maximum is reached quicker. The role of the ZnS shell is to passivate the CdSe core. As the amount of time to reach maximum emissivity decreases, it can be concluded that the ZnS shell reaches its maximum effect quicker. An explanation for this is that a fundamental change in the particle core has occurred as a result of the indium chloride and no further improvements to the particle's emission are obtained by surface passivation. No correlation between the amount of indium added and the growth rate of the ZnS shell is observed, and the previous observation cannot be explained by the passivating material growing faster (see Supporting Information). The data shows that as the amount of indium increases the emission of the ensemble of quantum dots decreases; further data on quantum yields and amount of indium detected by nuclear activation analysis will be presented below.

The experiments represented in Figure 5 are designed to determine if the changes shown in Figure 4 are caused by indium (a) or chloride (b). In Figure 4A, 10 mol % of $In(CH_3)_3$ is used as a source of indium. The effects of using $In(CH_3)_3$ are dramatic: the first peak that forms at 460 nm is never observed. Instead, a single peak grows in and continually shifts to the red, eventually reaching 510 nm and stopping. When the temperature is increased and the ZnS shell is added, QDs grown with $In(CH_3)_3$ do not grow as large as those grown with $InCl_3$ or no indium present. Figure 5B shows the effects NaCl has on the heterogeneous growth. It should be noted that, in the NaCl experiment, the amount of NaCl added is equivalent to the number of moles of chlorine associated with 10 mol % of $InCl_3$. NaCl is selected because it is believed that the ionic radius mismatch between Na^+ and Cd^{2+} will either force Na^+ ions to the surface of the particles or cause their complete removal from the particles. Similarly to the synthesis where indium and chloride were excluded, both emission peaks persist during the low-temperature phase of the synthesis instead of the first eventually being consumed to provide growth material for the second peak. It will be shown later that, within the experi-

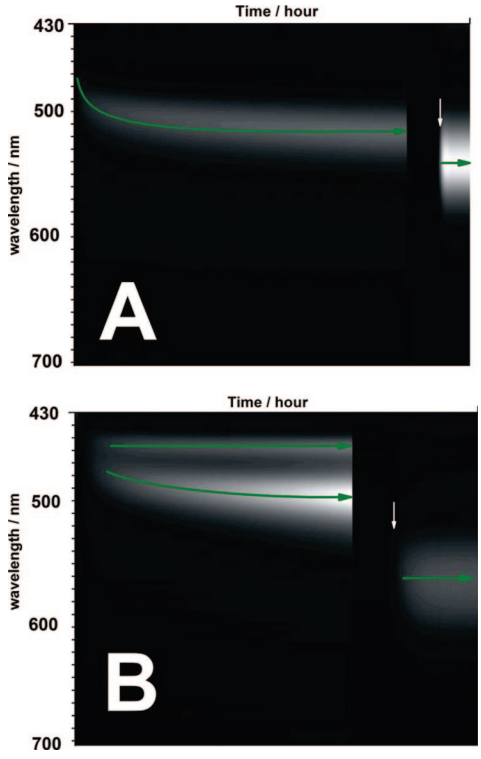

Figure 5. *In situ* photoluminescence of quantum dots during growth (A) doped with 10 mol % of $In(CH_3)_3$ with respect to cadmium and (B) growth in the presence of NaCl. The amount of NaCl used in (B) provides equal number of moles of Cl^- as present in 10 mol % of $InCl_3$. In the $In(CH_3)_3$ synthesis, the magic size nanocluster has a short lifetime, while in the NaCl synthesis, the magic size cluster remains through the entire low-temperature phase. The NaCl synthesis produces a more polydisperse sample, while the $In(Ch_3)_3$ has a smaller final size and a visibly higher final product emission.

ment time scale (~20 h), the NaCl experiment never reaches a maximum photoluminescence point at 460 nm, whereas all other experiments show a photoluminescence maximum reached some time during the low-temperature phase, indicating that the 460 nm peak is stabilized by the presence of NaCl. Also, after the ZnS shell is grown, it can be seen that the final particle emission spectrum is noticeably broader than that in all other experiments.

HRTEM images in Figure 6a−f are representative of particles grown by the method outlines in this paper. These specific quantum dots are taken from the 5 mol % of $InCl_3$ product. A wurtzite structure is clearly visible, though a white zig-zag line, representing the ABA-BAB... stacking sequence of the hexagonal basal planes, has been added to guide the viewer's eye. Figure 6G−J compiles XRD spectra of 5, 10, and 15 mol % doped quantum dots as well as the undoped sample. Each spectrum shows single crystal particles as well as the absence of InSe or In_2Se_3.

A more in-depth analysis of the effects of indium and chlorine on the growth of QDs is presented in Figure 7, showing the changes in normalized photoluminescence intensity at 460 nm with respect to time depending on the various doping agents and concentrations. As the concentration of $InCl_3$ increases, the maximum emission is reached quicker, while $In(CH_3)_3$ reaches a maximum emission almost immediately. Additionally, as the concentration of indium chloride increases, the emission at 460 nm decreases quicker, indicating that the magic sized nanoparticles producing emission at 460 nm are removed faster in the presence of indium. The addition of NaCl causes the ensemble to never reach a maximum emission within the time frame of the experiment (~20 h); rather it begins to steadily climb, indicating that NaCl actually stabilizes the particles against further growth. Final proof can be seen in the $In(CH_3)_3$ line as it drops off almost immediately once reaching a maximum emission intensity.

Figure 8A shows the maximum position of the second peak with respect to time. All of the syntheses follow a similar trend, in which the rate of growth has slowed considerably by the fifth hour. The amount of $InCl_3$ or $In(CH_3)_3$ alters the growth rate until the fifth hour, the 10 mol % of $In(CH_3)_3$ grows quickest during the initial hours, while the growth rate increases with increasing mol % of $InCl_3$. QDs grown without dopant or with NaCl display virtually the same growth rate, which is significantly slower than QDs grown with doping agents present. Combining the information given in Figures 7 and 8A, a compelling case can be made that the addition of a doping agent activates the particle surface to further growth. The trend in growth rate provided by Figure 8A corresponds to the trend in maximum emission time at 460 nm, the faster growing particles reach a maximum emission at 460 nm quicker.

Figure 8B shows the relationship between the full width at half-maximum of the second peak with respect to time and the type and concentration of the doping agent in meV. When the 450 nm peak reaches its maximum intensity in Figure 7, the second peak reaches its narrowest fwhm (Figure 8B), providing evidence that a size focusing takes place. This holds true for all experiments discussed here, except for the NaCl synthesis, which never reaches a maximum intensity at 460 nm. Again, combining Figure 5 with Figure 7B provides still more proof that the presence of indium activates particle growth. The fwhm minimum shown in Figure 8B corresponds to the period of time in Figure 7, where the emission at 460 nm is decreasing. This indicates that, once a maximum emission at 460 nm is reached, the smaller particles are consumed to provide monomers for the larger particles. There is also a relationship between the growth rates (Figure 8A) and the minimum of the fwhm, where the minimum fwhm corresponds to the approximate time the growth rate of the second peak begins to curtail. At this point, the monomer concentration in the solution has dropped below the critical concentration for colloid growth and Ostwald ripening begins to occur.

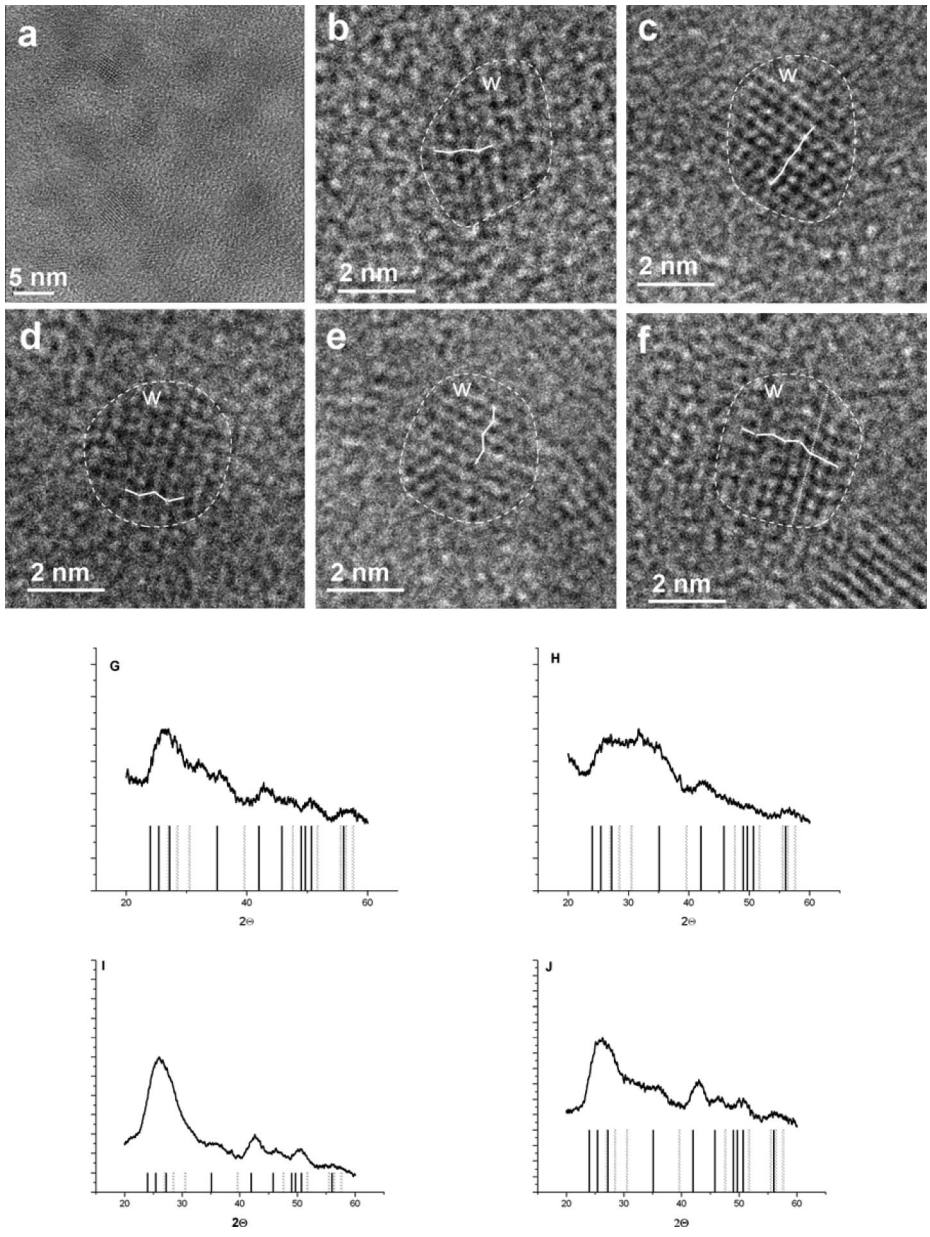

Figure 6. (a−f) HRTEM images of 5% $InCl_3$-doped CdSe core ZnS shell quantum dots. White zig-zag lines representing the ABABAB... stacking sequence have been added to guide the eye. Each particle shows a clear wurtzite crystal structure. (G−J) XRD spectrum of undoped, 5%, 10%, and 15% (respectively) $InCl_3$-doped core−shell quantum dots. Each spectrum shows a wurtzite CdSe (dark gray) crystal structure as well as peaks from the ZnS shell (light gray).

Analysis of the CdSe Nanoparticles. Table 1 summarizes the quantum yield of different batches of particles in relation to the amount and type of dopant added to the synthesis as well as the final peak position of the purified dots and the amount of ^{116}In detected by neutron activation. For clarification, the maximum emission position reported in Table 1 differs from those seen in the figures previously discussed: the *in situ* monitoring shows that the peak position at 250 °C and the peak position at room temperature are vastly different. This is due to the thermal excitation of the particles. As the particles cool, thermal energy is removed and the band edge sharpens due to fewer thermally excited phonons. The QY decreases when a doping agent is added and when NaCl is added. This is indicative of defects deep inside the particle caused by successful incorporation of indium or of surface traps caused by indium atoms bonded to the surface of the particles. It should be noted that these surface traps are caused by a defect atom and not a dangling bond and, therefore, cannot be eliminated with the growth of a ZnS shell on the particle surface and will continue to quench fluorescence after a passivating shell is grown. The syntheses with 10 and 15 mol % of $InCl_3$ have roughly the same quantum yield, suggesting that at 10 mol % the effects of indium chloride are maximized. The change in QY is greater moving from 10 to 5% and can be explained as a decrease in defects correlating to a decrease in available dopant. Interestingly, $In(CH_3)_3$ shows a far lower drop in QY compared to $InCl_3$, but the drop in QY of the NaCl batch is also far reduced from the undoped batch. Both indium and chloride ions effect the QY as seen from the NaCl and $In(CH_3)_3$ samples, with the NaCl having a more pronounced effect. If the quantum yield data from Table 1 are compared with the time evolution of the photoluminescence data in Figures 2–4, the conclusion is that the initial quantum yield of the nanoparticle at 120 °C is over 50%, which indicates high quality crystals present in the growth solution. The exception is the Me_3In data in Figure 4B, when the quantum yield is actually higher after growing the shell around the particle compared to the low-temperature growth data.

Table 1 contains the data regarding the effects of indium doping on the nucleation of QDs. The concentration of particles is calculated by the method outlined by Yu.[24] First, the calculated diameters of the particles differ as explained earlier. Second, all of the concentrations of QDs are within 10% of the mean value, indicating that adding indium or chlorine does not change the nucleation of particles grown by this method. Failure to alter the nucleation pattern indicates that this

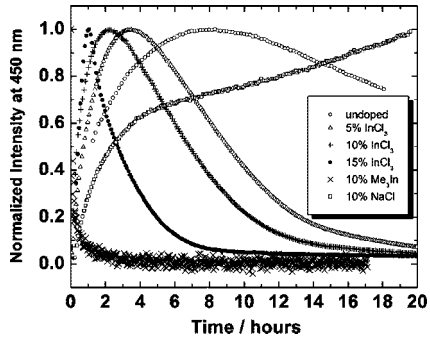

Figure 7. Normalized emission of the magic size cluster with respect to time in the presence and absence of various dopants used in the experiments. The emission of the $In(CH_3)_3$ sample reaches an immediate maximum and decreases rapidly, while the $InCl_3$ profiles reach maximums quicker and decrease quicker with increasing indium load. NaCl stabilizes the magic size cluster.

method does not create more highly energized nuclei that would alter the growth kinetics, and that the indium and chloride ions are responsible. If indium or chlorine were to effect the nucleation, significant deviation in the concentration of the particles would be expected, indicating that smaller or larger nuclei are required to begin the growth phase.

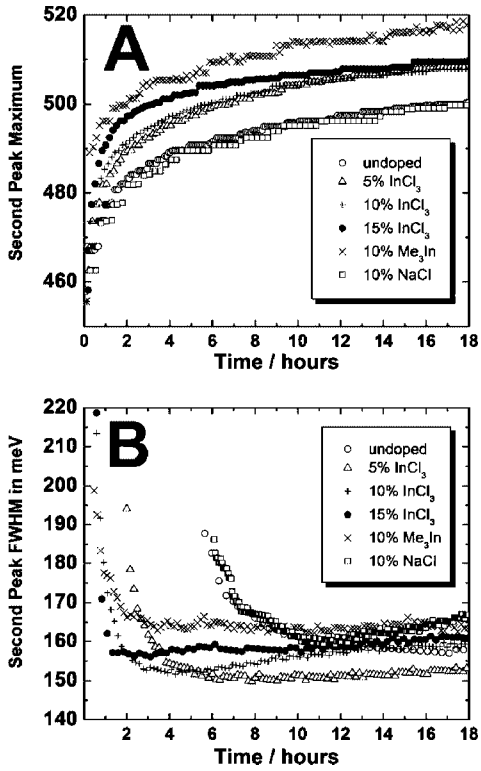

Figure 8. (A) Position of the second peak maximum with respect to time in the presence and absence of various dopants used in the experiments. Increasing the dopant load increases the growth rate of the second peak. $In(CH_3)_3$ produces larger particles during the low-temperature growth phase than $InCl_3$. It is also seen that $InCl_3$-doped particles all reach virtually the same size. (B) The fwhm of the second peak with respect to time. In all of the experiments represented in (B), the narrowest fwhm corresponds to the time of maximum emission shown in Figure 5, with the exception of the NaCl experiment, which never reaches a maximum in Figure 5.

Nuclear activation is used to detect whether or not indium is successfully incorporated into the QDs. Crude material was purified eight times through the MeOH/toluene process. After eight washes, the articles were no longer soluble in toluene, indicating the amine surface ligands had fallen off. Loss of surface ligands ensures that any indium located on the surface of the ZnS shell is washed away. The mol % detected for the 15% $InCl_3$ sample shows that there is no relationship between the mol % added to the system and the amount of indium detected, as the amount of indium detected for the 15 mol % sample is lower than the amount detected for the 10 mol % sample. There does appear to be a correlation between the amount of indium detected and the quantum yield, as the quantum yield decreases the amount of indium detected increases. This suggests that indium doping quenches fluorescence.

Pyridine ligand exchange was shown to remove Mg^{2+} surface-bound atoms,[25] and the same technique is used here to remove any surface-bound indium atoms. After refluxing the particles for 2 h in pyridine and precipitation with hexanes, nuclear activation data show no observable loss of indium atoms within the experimental error (20%). This indicates the vast majority of the indium atoms are deep enough in the particle that they are not lost during pyridine exchange. It is clear from these data that indium atoms incorporated into the quantum dots are retained through surface ligand exchange.

Figure 9 shows the absorption and emission spectra of the purified samples. The absorption and emission features of the $InCl_3$ samples are very narrow. The fwhm of the emission peak is approximately 120 $\pm$ 5 meV for all three $InCl_3$ samples. This is a significant improvement over 160 meV in Figure 8B after the 18 h reaction at 120 °C. The narrowing emission peak strongly suggests that there is a second focusing stage when the temperature is increased to 240 °C. The second focusing stage may be the result of the further activation of the remaining precursor fragment producing high monomer concentration. The width of the peak is still broad compared to the best literature result.[23] The undoped and the NaCl samples show complex emission and absorption structures. This is the result of an aggregated type of growth of the magic sized nanoparticles still present after 18 h of reaction at 120 °C and the second size.[19] It is noted also that the Me_3In sample also shows double peak behavior, which suggests a second nucleation step leading to aggregated type of growth.

Growth Model. The general growth model for the effects of indium doping during the low-temperature growth phase is depicted in Figure 10A. The figure only shows the relationship between the monomer exchange of the magic size nanoparticle and the solution. The top image represents the growth when no

TABLE 1.

experiment	QY	final PL peak position (nm)	indium detected (mol %)	λ_{abs}	diameter (nm)	concentration mol/L	In atoms per QD	In atoms per QD after pyridine exchange
no indium	27%	532	ND	517	5.11	1.13×10^{-6}	0	0
5% $InCl_3$	10.7%	563	0.40	550	5.79	9.53×10^{-7}	7.5	6.5
10% $InCl_3$	7.9%	571	0.49	558	6.00	1.06×10^{-6}	10.1	12.3
15% $InCl_3$	8.2%	581	0.44	572	6.43	9.62×10^{-7}	11.3	9.2
10% Me_3In	17.9%	504/519	NA	506	4.93	1.08×10^{-6}	NA	NA
30% NaCl	12.7%	543(shoulder)/558	NA	526	5.27	1.31×10^{-6}	NA	NA

dopant is present. The monomers released from the single source precursor molecule readily form the magic sized nanoclusters. Due to the increasing monomer concentration at the beginning of the growth, the concentration of the magic size nanoparticles increases. At the same time, the larger nanoparticles continue to grow and their size distribution focuses. Once the monomer concentration drops below the solubility limit, the size distribution of the nanoparticle increases and the nanoparticle growth significantly slows down (see Figure 8). The second scheme shows how adding indium to the particle surface accelerates the dissolution of MSNC to monomers. This results in a growth that occurs much faster because of the alteration of the surface energy caused by placing a +3 ion instead of a +2 ion. This may also cause a stronger bond for the next monomer, so that the rate of monomer attaching to the surface far exceeds the rate of monomers falling off the particle surface, which would explain why the $In(CH_3)_3$ reaction proceeds so fast that the MSNC is almost not observed. Last, the scheme shows how the chlorine ions actually stabilize the MSNC as observed in Figure 7. When the chloride ions bond to the particle surface, the rate of monomer exchange on the surface slows. It can be concluded that the indium atoms

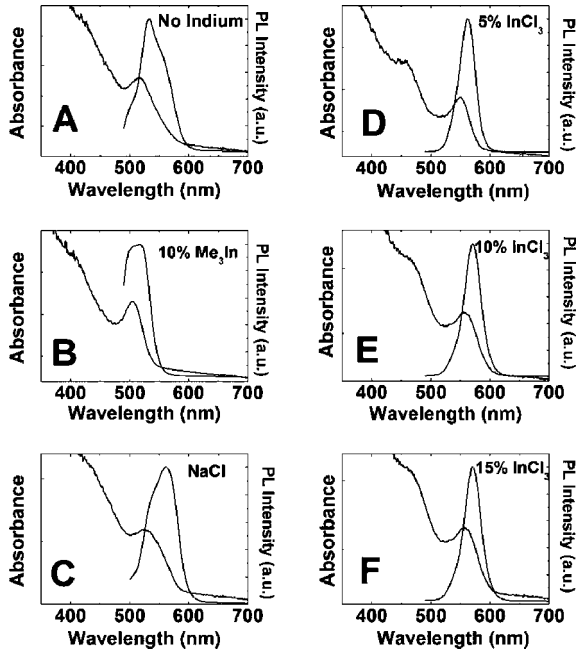

Figure 9. Normalized absorbance and photoluminescence profiles of isolated core/shell quantum dots in the presence and absence of various dopants used in the experiments. Experiments conducted with (D−F) $InCl_3$ produce a traditional Gaussian product distribution, while experiments with (B) $In(CH_3)_3$, (A) no dopant, and (C) NaCl yield a final product with two or more dominant sizes.

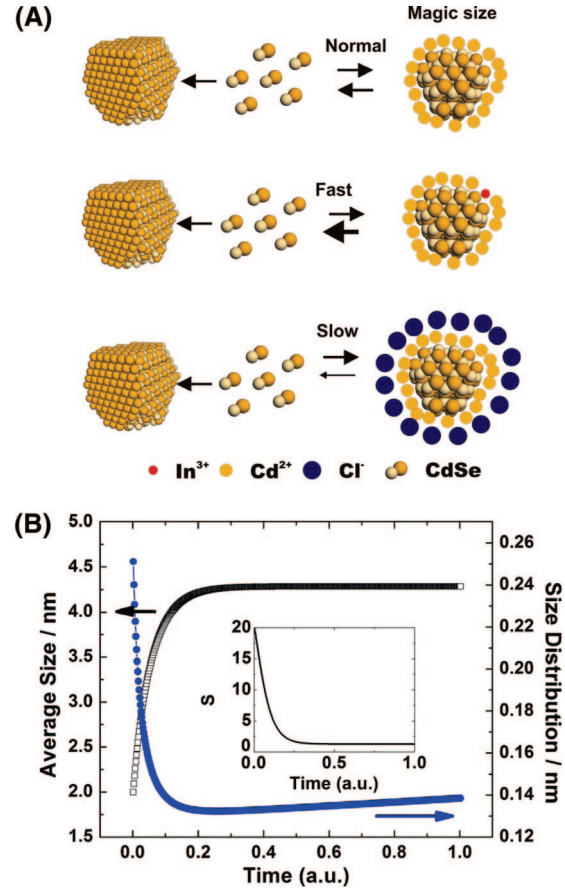

Figure 10. A proposed kinetic model of heterogeneous growth (A). Without the addition of any impurities, equilibrium is established between the dissolution of the magic size cluster and the free monomers in solution. Adding indium to the particle surface increases the rate of dissolution of magic size clusters to provide monomers for growth, while chloride ions stabilize the magic size cluster against dissolution. (B) The simulation of changes in size and size distribution of quantum dots (inset: supersaturation coefficient S as a function of time). The horizontal axis represents normalized time with the left vertical axis tracking the average particle size and the right vertical axis tracking the size distribution of the ensemble. In the inset, S reaches a minimum limit of $S = 1$ at approximately 0.20 time units, and the average size reaches a limit indicating growth has halted or slowed. At $t > 0.20$, the size distribution begins to increase as a result of the depletion of monomers from solution.

have a greater effect on the growth kinetics; otherwise, the $InCl_3$ samples would not have a larger final size after the high-temperature growth phase. Also, when only indium is present, the rate of dissolution and growth rate to the second size is so fast that few monomers remain for the high-temperature growth phase. This explains why the final particle size is so much smaller. In the presence of a shoulder on the blue side of the spectrum—at the high-temperature growth phase—Ostwald ripening is more prominent when chlorine is present and acting to stabilize the MSNC. This stabilization ensures that, when the high-temperature growth phase begins, there are sufficient monomers left to prevent Oswald ripening from dominating the high-temperature phase.

Figure 10B shows a simulation of how the ensemble of CdSe QDs in the present synthesis evolves. The second peak in the experimental data is used to monitor the focusing and defocusing of the particles. The details of the simulation are described elsewhere.[26] The inset of the graph shows that initially there is high monomer concentration present in the reaction mixture represented by *S*, which is the supersaturation of the monomer. As long as high concentration of monomers is present, the average QD size increases and the size distribution becomes narrower. The relatively long supersaturation can be explained by the presence of the small clusters, which results in higher solubility of the monomer and, therefore, larger supersaturation. Once the parameter *S* approaches 1, Ostwald ripening takes over the process. Initially, no significant change in average size takes place, but the size distribution becomes broad. Qualitatively, these data fit very well with the data presented in Figure 7.

The simulation assumes an initial size distribution to calculate the evolution of an ensemble of nanoparticles. The simulation predicts that the initial distribution will focus over time. If we take the magic size nanoparticle size distribution (fwhm = ~80 meV) as the initial distribution, a narrower emission is expected for the second peak. The observed initial distribution for the second peak is close to 200 meV, which seems contradictory. If the nucleation event is not instantaneous, than the broad initial distribution can explain the observed broadening. Although the theory can give reasons for the broadening, the physical meaning of this broadening remains to be explained. Potentially, if the nucleation event in this synthesis can be controlled, the synthesis could yield high quality nanoparticles *via* seeded growth.

A recent article by Knox *et al.*[27] concluded that indium doping does not change the optical properties of CdSe quantum dots, that the vast majority of the incorporated indium is present on the surface of the particles, and that no correlation exists between the amount of indium added to the synthetic system and the amount of indium detected by ICP elemental analysis or the degree to which photoluminescence is quenched.

Particles synthesized in the Knox report are created using a hot injection method where the doping agent ($InCl_3$) is injected simultaneously with the TOP:Se at the time of nucleation, and a ZnS shell is grown on several batches of particles. Introducing the dopant during the nucleation injection can result in amorphous In_2Se_3 forming, which would not show up in XRD or SAED studies. Also the mole ratios of Cd:In are so small in this report it is possible that an undetectable amount (by XRD) of this material is created. Finally, it is possible that trace amounts of In_2Se_3 remain in the quantum dots sample even after extensive washing.

The use of a single source precursor such as the one used to produce the results reported here is preferable to a hot injection method. In the single source precursor method, the cadmium and selenium are already bonded together in very small clusters and the growth system is cadmium-rich. This environment allows for the indium atoms present to bond directly to a preformed CdSe cluster. The cadmium-rich conditions also prevent the formation of a separate amorphous or crystalline indium containing particles, in fact cadmium-rich conditions might aid doping in this case by "soaking up" some of the chloride ions. However, at this time, it has not been possible to determine the location of the indium within the particles. Because the emission properties of (CdSe)ZnS core−shell quantum dots are determined by the narrower band gap CdSe, it is most likely that the indium incorporated in the particles reported here is on the "surface" of the CdSe core, sandwiched between CdSe and ZnS.

Like the Knox report, our results do not show a significant change in Stoke's shift or fwhm from particles grown without indium present and those grown in the presence of indium. All of the differences reported here, such as peak shape and position, can be explained by changes in size of the particles. Unlike the report by Knox *et al.*, the results presented here suggest a correlation between the amount of indium detected by nuclear activation and the quantum yield of the particles.

CONCLUSIONS

This study has shown that particles of significantly different size can coexist in a colloid system. It was previously believed that only one "family" of particles, centered about a single average size, could exist and that growth occurred in a stepwise manner from family to family. Here it is clearly seen that two distinctly different families can exist simultaneously. When various doping agents are introduced, the growth and dissolution rates of the particles change. The addition of indium as a doping agent effects not only the optical properties of the

nanocrystals but also their growth kinetics. Indium is found to activate the smaller MSNC to further growth, while chloride was shown to stabilize the MSNC against further growth. Both indium and chlorine are found to effect the quantum yield of the particles, and nuclear activation verified the presence of indium in the quantum dots after all growth phases were completed. The presence of indium indicated that some of the indium is retained by the quantum dots. At this time, it is not possible to determine the location of the indium atoms, but strong evidence exists to support their location being in the top most layers of the CdSe core.

EXPERIMENTAL SECTION

Chemicals. Selenium powder, acetonitrile, methanol, toluene, thiophenol, triethylamine, $InCl_3$, $Cd(NO_3)_2 \cdot 4H_2O$, $Li(NO_3)$, diethylzinc, $S(TMSi)_2$, and $In(CH_3)_3$ were used as purchased. Hexadecylamine (HDA) and trioctylphosphine (TOP) were distilled under vacuum with the second fraction collected and stored in a glovebox under N_2 atmosphere in the case of TOP, while HDA was stored on the shelf. The $Li_4[Cd_{10}Se_4(SPh)_{16}]$ precursor molecule was prepared by the method described by Cumberland *et al.*[17]

Synthesis of CdSe Quantum Dots. The method used to synthesize In-doped CdSe QDs is similar to the method described by Magana *et al.*[16] Briefly, 0.02 g (0.1 mmol) of $InCl_3$ was loaded into the flask shown in Figure 1 along with a magnetic stir bar in the glovebox. Twenty-five grams of HDA was added, followed by 0.3 g (1 mmol) of the $Li_4[Cd_{10}Se_4(SPh)_{16}]$ precursor molecule. Under Ar flow, the flask was gently heated until all of the HDA had melted (~40−50 °C). At this point, the *in situ* absorbance and photoluminescence equipment discussed below were set up for recording and the setup was covered in tin-foil to reduce heat loss. The temperature was increased to 120 °C, and the reaction was stirred overnight under Ar flow. For the experiments where trimethylindium was used as the doping agent, the appropriate amount of trimethylindium was dissolved in ~3 mL of TOP and injected once the HDA had melted and the temperature was set to 150 °C to ensure decomposition of the complex and left overnight. Approximately 16−18 h later, the temperature was increased to 240 °C for 3 h to allow further growth. Afterwards, the temperature was increased to 250 °C and 4 mL of a Zn/S/TOP stock solution containing 7.5 mL of diethylzinc and 0.75 mL of hexamethyldisilithane diluted in 30 mL of distilled TOP was added over 5 min, and the reaction was left at 250 °C for 1 h to allow for shell growth. Upon cooling, the crude material was centrifuged to remove metallic zinc. Further purification was achieved by precipitation of (CdSe)ZnS particles with MeOH followed by further centrifugation. The supernatant was discarded and the QDs dispersed in toluene. A final precipitation with methanol followed by centrifugation and dispersion in toluene completed the purification process.

***In Situ* Monitoring of Absorbance and Photoluminescence.** Figure 1 shows the flask and equipment used for the *in situ* monitoring of the absorbance and the photoluminescence of the quantum dots. The experimental details of the *in situ* absorption spectroscopy used in the experiments are previously described.[19] Briefly, a 1 mm path length cuvette was attached to the reaction vessel. The hot solution continuously flowed through the cuvette, which allowed monitoring of the absorbance of the growth solution. The path length of the cuvette was optimized to ensure optimum mixing in the cuvette and to achieve the desired optical density. A fiber optic absorption spectrometer was used to obtain the absorbance spectra. A separate fiber optic fluorescence spectrometer was utilized to acquire the photoluminescence spectra of the reaction mixture. A fluorescence Raman probe equipped with a 395 nm excitation wavelength LED was used to collect photoluminescence. The photoluminescence probe was situated as close to the reaction flask as possible and positioned so as to maximize the amount of signal collected. The amount of the fluorescence collected from the reaction flask was varied from reaction to reaction as well as the positioning of the Raman probe. However, the relative changes of the fluorescence during growth remained constant. The back-reflected excitation source intensity allowed for monitoring of the stability of the fluorescence setup, which remained constant throughout the experiment.

Acknowledgment. The authors would like to acknowledge Kansas State University and the Department of Chemistry at Kansas State University for the funding. The Imaging and Microscopy Facility at the University of California, Merced, is gratefully acknowledged for the use of its instruments. The Kansas State University Nuclear Research Reactor is also gratefully acknowledged for their help with the nuclear activation experiments.

Supporting Information Available: In situ photoluminescence of CdSe quantum dots from $Li_4[Cd_{10}Se_4(SPh)_{16}]$ complex during growth at 120 °C over a 24 h period, indicating the three main growth stages of the synthesis: (a) nucleation, (b) heterogeneous growth of the particles, and (c) increase of the temperature and the growth of the ZnS shell. This material is available free of charge via the Internet at http://pubs.acs.org.

REFERENCES AND NOTES

1. Murray, C. B.; Norris, D. J.; Bawendi, M. G. Synthesis and Characterization of Nearly Monodisperse CdE (E = S, Se, Te) Semiconductor Nanocrystallites. *J. Am. Chem. Soc.* **1993**, *115*, 8706–8715.
2. Peng, X. G.; Manna, L.; Yang, W. D.; Wickham, J.; Scher, E.; Kadavanich, A.; Alivisatos, A. P. Shape Control of CdSe Nanocrystals. *Nature* **2000**, *404*, 59–61.
3. Manna, L.; Milliron, D. J.; Meisel, A.; Scher, E. C.; Alivisatos, A. P. Controlled Growth of Tetrapod-Branched Inorganic Nanocrystals. *Nat. Mater.* **2003**, *2*, 382–385.
4. Peng, X. G.; Schlamp, M. C.; Kadavanich, A. V.; Alivisatos, A. P. Epitaxial Growth of Highly Luminescent CdSe/CdS Core/Shell Nanocrystals with Photostability and Electronic Accessibility. *J. Am. Chem. Soc.* **1997**, *119*, 7019–7029.
5. Dabbousi, B. O.; RodriguezViejo, J.; Mikulec, F. V.; Heine, J. R.; Mattoussi, H.; Ober, R.; Jensen, K. F.; Bawendi, M. G. (CdSe)ZnS Core−Shell Quantum Dots: Synthesis and Characterization of a Size Series of Highly Luminescent Nanocrystallites. *J. Phys. Chem. B* **1997**, *101*, 9463–9475.
6. Nozik, A. J. Quantum Dot Solar Cells. *Physica E* **2002**, *14*, 115–120.
7. Medintz, I. L.; Uyeda, H. T.; Goldman, E. R.; Mattoussi, H. Quantum Dot Bioconjugates for Imaging, Labelling and Sensing. *Nat. Mater.* **2005**, *4*, 435–446.
8. Norris, D. J.; Efros, A. L.; Erwin, S. C. Doped Nanocrystals. *Science* **2008**, *319*, 1776–1779.
9. Yu, D.; Wang, C. J.; Guyot-Sionnest, P. n-type Conducting CdSe Nanocrystal Solids. *Science* **2003**, *300*, 1277–1280.
10. Galli, G. Solid-State physics—Doping the Undopable. *Nature* **2005**, *436*, 32–33.
11. Dalpian, G. M.; Chelikowsky, J. R. Self-Purification in Semiconductor Nanocrystals. *Phys. Rev. Lett.* **2006**, 96.
12. Archer, P. I.; Santangelo, S. A.; Gamelin, D. R. Direct Observation of sp-d Exchange Interactions in Colloidal Mn^{2+}- and Co^{2+}-Doped CdSe Quantum Dots. *Nano Lett.* **2007**, *7*, 1037–1043.
13. Hanif, K. M.; Meulenberg, R. W.; Strouse, G. F. Magnetic Ordering in Doped $Cd_{1-x}Co_xSe$ Diluted Magnetic Quantum Dots. *J. Am. Chem. Soc.* **2002**, *124*, 11495–11502.
14. Levy, M.; Lee, W. K.; Sarachik, M. P.; Geschwind, S.

Photoluminescence of Heavily Doped N-Type CdSe. *Phys. Rev. B* **1992**, *45*, 11685–11692.
15. Perna, G.; Capozzi, V.; Minafra, A.; Pallara, M.; Ambrico, M. Effects of the Indium Doping on Structural and Optical Properties of CdSe Thin Films Deposited by Laser Ablation Technique. *Eur. Phys. J. B* **2003**, *32*, 339–344.
16. Magana, D.; Perera, S. C.; Harter, A. G.; Dalal, N. S.; Strouse, G. F. Switching-On Superparamagnetism in Mn/CdSe Quantum Dots. *J. Am. Chem. Soc.* **2006**, *128*, 2931–2939.
17. Cumberland, S. L.; Hanif, K. M.; Javier, A.; Khitrov, G. A.; Strouse, G. F.; Woessner, S. M.; Yun, C. S. Inorganic Clusters as Single-Source Precursors for Preparation of CdSe, ZnSe, and CdSe/ZnS Nanomaterials. *Chem. Mater.* **2002**, *14*, 1576–1584.
18. Talapin, D. V.; Rogach, A. L.; Shevchenko, E. V.; Kornowski, A.; Haase, M.; Weller, H. Dynamic Distribution of Growth Rates Within the Ensembles of Colloidal II−VI and III−V Semiconductor Nanocrystals as a Factor Governing their Photoluminescence Efficiency. *J. Am. Chem. Soc.* **2002**, *124*, 5782–5790.
19. Dagtepe, P.; Chikan, V.; Jasinski, J.; Leppert, V. J. Quantized Growth of CdTe Quantum Dots; Observation of Magic-Sized CdTe Quantum Dots. *J. Phys. Chem. C* **2007**, *111*, 14977–14983.
20. Peng, Z. A.; Peng, X. G. Nearly Monodisperse and Shape-Controlled CdSe Nanocrystals *via* Alternative Routes: Nucleation and Growth. *J. Am. Chem. Soc.* **2002**, *124*, 3343–3353.
21. Chikan, V.; Kelley, D. F. Size-Dependent Spectroscopy of MoS_2 Nanoclusters. *J. Phys. Chem. B* **2002**, *106*, 3794–3804.
22. Leff, D. V.; Ohara, P. C.; Heath, J. R.; Gelbart, W. M. Thermodynamic Control of Gold Nanocrystal Size—Experiment and Theory. *J. Phys. Chem.* **1995**, *99*, 7036–7041.
23. Qu, L. H.; Peng, X. G. Control of Photoluminescence Properties of CdSe Nanocrystals in Growth. *J. Am. Chem. Soc.* **2002**, *124*, 2049–2055.
24. Yu, W. W.; Qu, L. H.; Guo, W. Z.; Peng, X. G. Experimental Determination of the Extinction Coefficient of CdTe, CdSe, and CdS Nanocrystals. *Chem. Mater.* **2003**, *15*, 2854–2860.
25. Mikulec, F. V.; Kuno, M.; Bennati, M.; Hall, D. A.; Griffin, R. G.; Bawendi, M. G. Organometallic Synthesis and Spectroscopic Characterization of Manganese-Doped CdSe Nanocrystals. *J. Am. Chem. Soc.* **2000**, *122*, 2532–2540.
26. Talapin, D. V.; Rogach, A. L.; Haase, M.; Weller, H. Evolution of an Ensemble of Nanoparticles in a Colloidal Solution: Theoretical Study. *J. Phys. Chem. B* **2001**, *105*, 12278–12285.
27. Knox, C. K.; Fillmore, S. D.; Call, D. M.; Allen, D. G.; Hess, B. C.; Davis, R. C.; Evenson, W. E.; Harrison, R. G. Synthesis and Characterization of Photoluminescent In-doped CdSe Nanoparticles. *J. Colloid Interface Sci.* **2006**, *300*, 591–596.